A Unified Statistical/Deterministic Deformable Model for LV Segmentation in Cardiac MRI

Sharath Gopal and Demetri Terzopoulos

Computer Science Department
University of California, Los Angeles, USA

Abstract. We propose a novel deformable model with statistical and deterministic components for LV segmentation in cardiac magnetic resonance (MR) cine images. The statistical deformable component learns a global reference model of the LV using Principal Component Analysis (PCA) while the deterministic deformable component consists of a finite-element deformable surface superimposed on the reference model. The statistical model accounts for most of the global variations in shape found in the training set while the deterministic skin accounts for the local deformations consistent with the detailed image features. Intensity gradient-based image forces are applied to the model to segment and reconstruct LV shape. We validate our model on the MICCAI Grand Challenge dataset using leave-one-out training. Comparing the automated segmentation to the manual segmentation yields a Mean Perpendicular Distance (MPD) of 3.65 mm and a Dice coefficient of 0.86.

1 Introduction

The myocardial wall in the left ventricle (LV) is the main pumping structure of the heart and its function is important in the assessment of cardiovascular disease. By accurately segmenting the LV in cine MR images, cardiac contractile function can be quantified according to LV volumes and ejection fractions. Manual segmentation in MR images is a tedious process performed by clinicians, which is subject to inter- and intra-observer variability that can lead to inconsistent diagnosis. These issues have motivated researchers to develop automated methods that aspire to match the ability of expert clinicians to segment LV shape. The recent survey [1] provides an overview of different methods that have been applied to LV segmentation in MR images.

Deformable models have revolutionized model-based image analysis and their variational approach has been successfully applied to segmentation and tracking in medical images [2]. For example, the deformable model in [3] involves a regularization energy, which controls smoothness of the surface, and an image energy, which is generated from image features. The shape of the surface evolves under the influence of external forces to attain a minimum-energy configuration. Such models provide local control over the surface and include only weak shape priors that impose anatomical constraints yielding smooth, closed LV shapes in MR short axis images.

The Deformable Superquadric Model (DSM) formulation in [4] includes a stronger shape prior in the form of a global superquadric shape. A finite-element locally deformable skin is superimposed on this global parameterized reference shape. The global and local degrees of freedom of the deformable model evolve under the influence of external forces, leading to the optimal fit of the reference shape and skin. As we show in the present paper, this formulation is appropriate for introducing statistically learned global reference shapes.

The statistical deformable model-based analysis of images was pioneered by the introduction of the Active Shape Model (ASM) [5] and the Active Appearance Model (AAM) [6], which use Principal Component Analysis (PCA) to learn appropriate shape/deformation priors from hand-segmented data. The AAM has been successfully applied to LV segmentation from cardiac MR images [7–10]. These methods provide a strong prior for shape and texture, such that the resulting shape is influenced by the variations present in the training set. PCA-based methods provide global control of shape and appearance, but the PCA priors can often be too restrictive and may not generalize well to variations not observed in the training set. Such uncommon variations can occur in pathological cases such as myocardial infarction and cardiomyopathy.

The above considerations have motivated our efforts to combine statistical and deterministic deformable models. In [11] we combined AAMs and DSMs in a multi-model, multi-stage approach. In the present paper, we further develop our approach by proposing a novel unified deformable model that replaces the superquadric reference shape with a statistically-learned PCA reference shape.

With similar motivations, a PCA shape prior is embedded in the internal energy formulation of a deformable mesh in [13]. At each iteration, the internal energy is dictated by the projection of the resulting shape on the modes of variation. The gradient-based data term is part of the external energy, and is responsible for pulling the mesh towards features of interest. Our model is more generic in the sense that any kind of external forces (gradient, inertial, or optical flow) can be applied to influence shape without any change to the model's formulation. The PCA parameters evolve simultaneously along with the pose and local displacement parameters, all under the influence of external forces. Such abstraction of external forces facilitates the design of image potential functions that influence the shape of the model. For example, we can design a potential based on optical flow to change the shape of the model according to the LV motion across phases in the images. Finally, the finite element skin provides good control over the smoothness of the surface, and by virtue of its ability to evolve independently, it is able to assume shapes that may not have been captured by the learned deformations of the PCA reference shape.

2 Model Formulation

Our formulation combines the strengths of deterministic and statistical deformable models. On the one hand, a PCA statistical component provides a strong learned shape prior that captures the global variations in the training

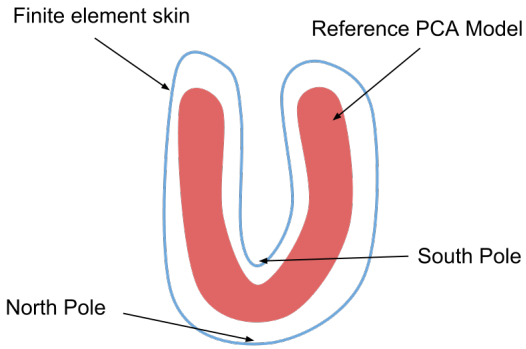

Fig. 1. Model Geometry

set. On the other hand, a deterministic deformable component affords local variations in shape that are dictated by the observed image features. The formulation of our model mainly involves embedding the PCA reference as illustrated in Fig. 1.

2.1 Geometry

The model is a closed surface that has $\mathbf{u} = (u, v)$ as its material coordinates. Principal Component Analysis (PCA) is applied to a set of aligned 3D LV shapes to obtain a discrete reference shape $\mathbf{s}(\mathbf{u})$ as

$$\mathbf{s}(\mathbf{u}) = \bar{\mathbf{s}}(\mathbf{u}) + \mathbf{P}_s(\mathbf{u})\mathbf{q}_s(\mathbf{u})^T, \tag{1}$$

where $\bar{\mathbf{s}}$ is the mean shape, the columns of matrix $\mathbf{P}_s$ are the modes of variation, and $\mathbf{q}_s$ are the shape or the PCA parameters. The translational offsets across the training shapes are removed by translating the respective centroids to the origin, and the rotational offsets are removed using Ordinary Procrustes Analysis. The Jacobian of the PCA reference shape $\mathbf{s}$ is given by

$$\mathbf{J}(\mathbf{u}) = \frac{\partial \mathbf{s}(\mathbf{u})}{\partial \mathbf{q}_s(\mathbf{u})} = \mathbf{P}_s(\mathbf{u}), \tag{2}$$

thus characterizing how the shape changes when the parameters $\mathbf{q}_s$ change. The Jacobian is key to the interaction of external forces with the model dynamics described later.

A finite element deformable skin is superimposed on the reference shape (Fig. 2) to account for local deformations. The local displacements $\mathbf{d}(\mathbf{u})$ are expressed as a linear combination of finite element basis functions $\mathbf{b}_i(\mathbf{u})$ as follows:

$$\mathbf{d}(\mathbf{u}) = \sum_i \mathrm{diag}(\mathbf{b}_i(\mathbf{u}))\mathbf{q}_i = \mathbf{S}\mathbf{q}_d, \tag{3}$$

where $\mathbf{q}_d = (..., \mathbf{q}_i, ...)^T$ is a set of local displacements $\mathbf{q}_i$ at each mesh node i and $\mathbf{S}$ holds the basis functions. In addition to the PCA parameters $\mathbf{q}_s$ and the local displacement parameters $\mathbf{q}_d$, the unified model also has global translation and rotation parameters $\mathbf{q}_c$ and $\mathbf{q}_\theta$. All the degrees of freedom (DOF) for the model are collected in a single vector

$$\mathbf{q} = (\mathbf{q}_c^T, \mathbf{q}_\theta^T, \mathbf{q}_s^T, \mathbf{q}_d^T)^T. \tag{4}$$

2.2 Dynamics

Given a new set of MR image slices for a patient, the vector $\mathbf{q}$ yielding a model that best fits the images must be computed. Applying Lagrangian dynamics, the model is made dynamic in $\mathbf{q}$, thus characterizing the evolution of $\mathbf{q}$ under the influence of external forces. The equations of motion are given as

$$\mathbf{C}\dot{\mathbf{q}} + \mathbf{K}\mathbf{q} = \mathbf{f}_q, \tag{5}$$

where $\dot{\mathbf{q}}$ is the time derivative of the DOF, $\mathbf{C}\dot{\mathbf{q}}$ are damping forces, $\mathbf{K}\mathbf{q}$ are elastic forces and $\mathbf{f}_q$ are external forces applied to the model. The stiffness matrix $\mathbf{K}$ determines the material/elastic properties of the finite element skin.

We impose a spline deformation energy on the local displacements $\mathbf{q}_d$ as

$$E(\mathbf{d}) = \int w_1(\mathbf{u}) \left(\left(\frac{\partial \mathbf{d}}{\partial u} \right)^2 + \left(\frac{\partial \mathbf{d}}{\partial v} \right)^2 \right) + w_0(\mathbf{u})\mathbf{d}^2 \, du \, dv, \tag{6}$$

where $w_0(\mathbf{u})$ controls the magnitude of the local deformation and $w_1(\mathbf{u})$ controls its variation across adjacent nodes on the skin.

The equations of motion in (5) are integrated through time using an explicit Euler method. The degrees of freedom in the vector $\mathbf{q}$ are updated from time t to time $t + \Delta t$ as follows:

$$\mathbf{q}^{(t+\Delta t)} = \mathbf{q}^{(t)} + \Delta t \Big(\mathbf{C}^{(t)} \Big)^{-1} \left(\mathbf{f}_q^{(t)} - \mathbf{K}\mathbf{q}^{(t)} \right). \tag{7}$$

Such a system will come to rest when the internal (damping and elastic) and external (image) forces equilibrate. Additional background details about the formulation and implementation are provided in [4].

2.3 Image Forces

The model, initialized with a mean PCA reference shape, is placed in the 3D volume formed by the MR slice stack, and deformed under the influence of image forces. The image forces are designed to attract the surface of the model towards the respective myocardial boundaries (endo and epi). The first step in designing forces is to define a gradient-based potential function on an image I as

$$P = \|\nabla(G_\sigma * I)\|, \tag{8}$$

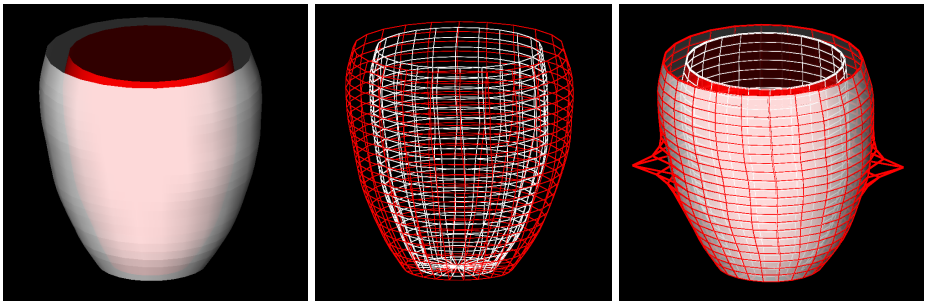

Fig. 2. PCA reference (left). Finite Element skin (center). Skin pulled away from the reference (right).

where the Gaussian smoothing width σ determines the range of influence of the forces. Multiple smoothing widths (Fig. 3) are used to attain equilibrium faster. Such a potential function presents image forces that attract the surface of the model towards image intensity edges. The force distribution is the gradient of the potential function:

$$\mathbf{f} = \beta \nabla P, \tag{9}$$

where β controls the scale of the force. The values for β, the stiffness parameters $w_1(\mathbf{u})$ and $w_0(\mathbf{u})$, and the time step Δt are carefully selected to maintain stability. In our implementation, we have used constant values $w_1 = 4 \times 10^{-3}$ and $w_0 = 2 \times 10^{-6}$, $\beta = 30$, and $\Delta t = 1$. The image smoothing and normalization methods affect the choice of these values.

We apply two different kinds of forces to the inner and outer walls of our model to differentiate between the endocardial wall (LV blood pool-myocardium interface) and the epicardial wall (myocardium/right ventricle (RV) and myocardium/outer organs interfaces). Since the blood pool and the pericardial fat appear bright and the myocardium appears dark in cine MR images, we can make use of the information present in the direction of the image gradients. At the endocardial border, the image gradients are oriented towards the LV blood pool, whereas at the epicardial border, the image gradients are oriented away from the LV blood pool. Thus, the endocardial forces $\mathbf{f}_{\text{I}}$ and the epicardial forces $\mathbf{f}_{\text{O}}$ are given as

$$\mathbf{f}_{\text{I}}(\mathbf{u}) = \begin{cases} \mathbf{f}(\mathbf{u}), & \text{if } \nabla I \cdot \mathbf{x}(\mathbf{u}) < 0 \\ 0, & \text{otherwise,} \end{cases} \tag{10}$$

$$\mathbf{f}_{\text{O}}(\mathbf{u}) = \begin{cases} \mathbf{f}(\mathbf{u}), & \text{if } \nabla I \cdot \mathbf{x}(\mathbf{u}) > 0 \\ 0, & \text{otherwise,} \end{cases} \tag{11}$$

where the tests involve the projection of the image gradient on the position vectors $\mathbf{x}(\mathbf{u})$ of the points on the model surface whose centroid is at the origin.

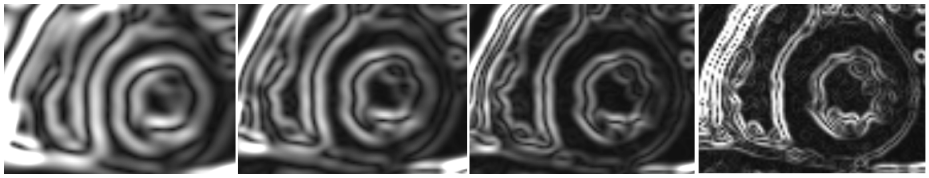

Fig. 3. Image potentials at multiple smoothing widths (4, 3, 2, 0 mm)

MPD	ED-Epi	ED-Endo	Dice	ED-Epi	ED-Endo
MEAN	3.6	3.7	MEAN	0.88	0.84
STD	0.52	0.62	STD	0.02	0.04
MAX	4.89	4.68	MAX	0.93	0.91
MIN	2.11	2.16	MIN	0.81	0.75

Table 1. Mean Perpendicular Distance (mm) and Dice coefficient (45 cases)

3 Results

We validated the segmentation ability of our model using leave-one-out training on end-diastolic (ED) images of the 45 MICCAI Grand Challenge datasets. The leave-one-out validation was fully automated and the mean reference model was initialized in the volume such that the centroid of the model coincided with the center of the mid-slice. Initially, the model was subject only to translational forces designed using optical flow potentials across phases. Such forces approximately localize the myocardium and help in moving the initial mean reference closer to the actual solution. Subsequently, all the parameters (rigid and non-rigid) were stepped forward in time. The PCA parameters $\mathbf{q}_s$ are restricted within $+2$ and -2 standard deviations (which can be obtained from the corresponding eigenvalues) from the mean in order to prevent unlikely shapes. The deformation of the skin is controlled by the w_1 and w_0 constants. The model is stepped forward across multiple Gaussian smoothing widths (4, 3, 2, 0 mm), finally converging at the myocardial boundaries.

Due to the ambiguous gradient information at the myocardium interface with lungs and other organs, the epicardial boundary is harder to localize. By virtue of the model having the MICCAI Grand Challenge trained PCA reference shape, the papillary muscles were included in the blood pool (Fig. 4). We used the Mean Perpendicular Distance (MPD) and Dice coefficients (Table 1) to compare the positioning errors of automated contours with respect to the expert-delineated contours. The average Dice coefficient and the average MPD for the ED segmentation are 0.86 and 3.65 mm respectively, and these are close to the results presented in [14], [15], and [16]. The automated contours for the mid-slices are

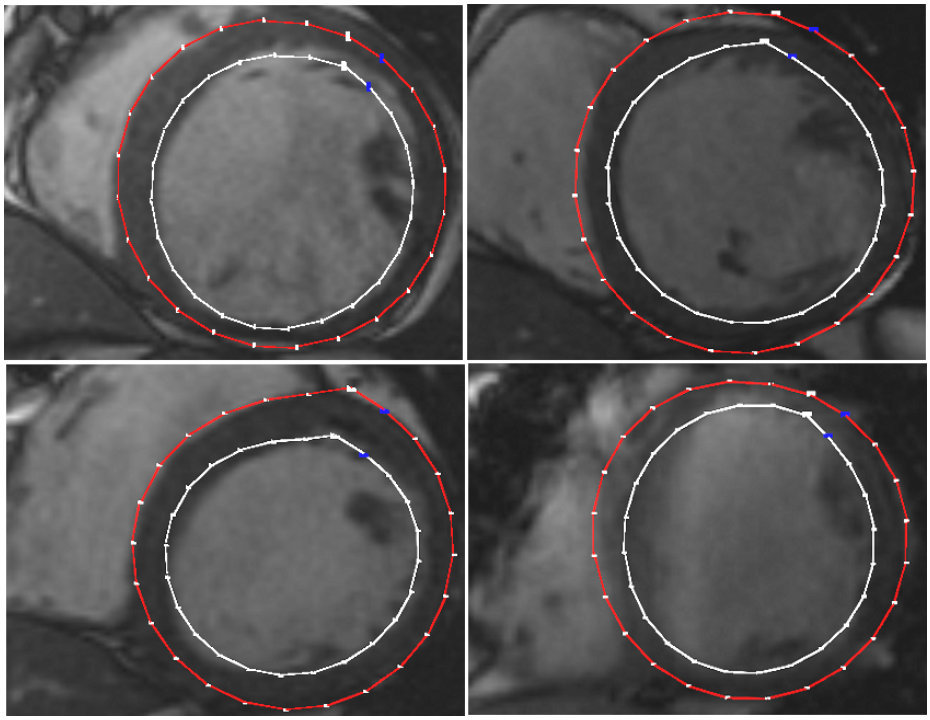

Fig. 4. Examples of automated contour segmentation for four cases

more accurate than those for the slices towards the apex due to partial volume effects.

4 Conclusion

We have proposed a novel deformable model for LV segmentation in cardiac MR images, which combines a strong statistical prior learned from manually-segmented training data through PCA with a finite element deformable skin. Our model is unique in the sense that the PCA reference shape is embedded in its physical formulation and it evolves under the influence of external image forces. Leave-one-out validation on the 45 MICCAI Grand Challenge datasets yields good results. Our work brings us a step closer to the automation of all phases of LV segmentation in cardiac cine MRI.

References

1. Petitjean, C., Dacher, J. A review of segmentation methods in short axis cardiac MR images. *Medical Image Analysis*, **15**, 169–184, (2011).

2. McInerney, T., Terzopoulos, D. Deformable models in medical image analysis: A survey. *Medical Image Analysis*, **1**(2), 91–108, (1996).
3. McInerney, T., Terzopoulos, D. A dynamic finite element surface model for segmentation and tracking in multidimensional medical images with application to 4-D image analysis. *Comp. Med. Imag. Grap.*, **19**(1), 69–83, (1995).
4. Terzopoulos, D., Metaxas, D.: Dynamic 3D models with local and global deformations: Deformable superquadrics. *IEEE Transactions on PAMI*, **13**(7), 703–714 (1991).
5. Cootes, T. F., Taylor, C. J., Cooper, D. H., Graham, J. Active shape models: Their training and application. *Comp. Vis. Imag. Understanding*, **61**, 38-59, (1995).
6. Cootes, T. F., Edwards, G. J., Taylor, C. J.: Active appearance models. *Proc. ECCV*, 484–498, (1998).
7. Mitchell, S. C., Bosch, J. G., Lelieveldt, B. P. F., van der Geest, R. J., Reiber, J. H. C., Sonka, M. 3D Active appearance models: Segmentation of cardiac MR and ultrasound images. *IEEE Transactions on Medical Imaging*, **21**(9), 1167–1178, (2002).
8. Mitchell, S. C., Lelieveldt, B. P. F., van der Geest, R. J., Bosch, H. G., Reiber, J. H. C., Sonka, M. Multistage hybrid Active Appearance Model matching: Segmentation of left and right ventricles in cardiac MR images. *IEEE Transactions on Medical Imaging*, **20**(5), 415–423, (2001).
9. Zhang, H., Wahle, A., Johnson, R.K., Scholz, T.D., Sonka, M. 4-D cardiac MR image analysis: Left and right ventricular morphology and function. *IEEE Transactions on Medical Imaging*, **29**(2), 350–364, (2010).
10. Stegmann, M. B., Perdersen, D. Bi-temporal 3D active appearance models with applications to unsupervised ejection fraction estimation. *Proc. of SPIE Medical Imaging*, 5747, 336–350, (2005).
11. Gopal, S., Otaki, Y., Arsanjani, R., Berman, D., Terzopoulos, D., Slomka, P.: Combining active appearance and deformable superquadric models for LV segmentation in cardiac MRI. *Proc. SPIE Medical Imaging*, 8669-15:1–8, (2013).
12. Radau, P., Lu, Y., Connelly, K., Paul, G., Dick, A. J., Wright, G. A.: Evaluation framework for algorithms segmenting short axis cardiac MRI. *The MIDAS Journal - Cardiac MR Left Ventricle Segmentation Challenge.* http://hdl.handle.net/10380/3070, (2009).
13. Kaus., M, Von Berg, J., Weese, J., Niessen, W., Pekar, V. Automated segmentation of the left ventricle in cardiac MRI. *Medical Image Analysis*, **8**(3), 245–254, (2004).
14. Jolly, MP., Fully automatic left ventricle segmentation in cardiac cine MR images using registration and minimum surfaces. *The MIDAS Journal—Cardiac MR Left Ventricle Segmentation Challenge*, (2009).
15. Huang, S., Liu, J., Lee, L., Venkatesh, S., Teo, L., Au, C., Nowinski, W. Segmentation of the left ventricle from cine MR images using a comprehensive approach. *The MIDAS Journal—Cardiac MR Left Ventricle Segmentation Challenge*, (2009).
16. Lu, Y., Radau, P., Connelly, K., Dick, A., Wright, G. Automatic image-driven segmentation of left ventricle in cardiac cine MRI. *The MIDAS Journal—Cardiac MR Left Ventricle Segmentation Challenge*, (2009).